RSC Advances

PAPER

View Article Online
View Journal | View Issue

CrossMark click for updates

Cite this: *RSC Adv.*, 2016, **6**, 53358

Fine tuning of molecular and supramolecular properties of simple trianglimines – the role of the functional group†‡

J. Gajewy,*[ab] J. Szymkowiak[ab] and M. Kwit*[ab]

Chiral, triangular poly-azamacrocycles (trianglimines) readily available from enantiomerically pure *trans*-1,2-diaminocyclohexane and various aromatic dialdehydes, differ in their nature and substitution pattern. The highly symmetrical macrocycle having two electron-donating groups attached to the aryl moieties is formed under thermodynamic control that fulfilled the so called entropy of symmetry rule. Conversely, from the 2-nitroterephthaldehyde a kinetic product of trivial C_1 symmetry is solely obtained, whereas from 2-methoxyterepthaldehyde a mixture of C_3- and C_1-symmetrical macrocycles are formed. The factors that contribute to the mechanism of the macrocycle formation were determined on the basis of an experimental/theoretical approach. The non-symmetrical structure of the macrocycle resulted from a symmetrical intermediate that appeared during cyclocondensation. The chiroptical properties of the trianglimines were studied by means of experimental ECD and VCD methods supported by quantum-chemical calculations. The nitro-substituted trianglimine appeared to be a simple, low molecular weight supergelator forming in polar media of stable chiral organogels. The structure of the gel is affected by the nature and chirality of the dopant. The hexaimine macrocycles after reduction of the C=N imine bonds formed trianglamines – useful chiral ligands in stereoselective synthesis. The Zn–trianglamine complexes were employed as catalysts for asymmetric hydrosilylation of prochiral ketones, providing products of enantiomeric excess up to 98%. This remains the best result obtained for Zn–diamine catalysed asymmetric hydrosilylation of ketones so far.

Received 7th March 2016
Accepted 23rd May 2016

DOI: 10.1039/c6ra06095a

www.rsc.org/advances

Published on 27 May 2016. Downloaded by UNIVERSITY OF NEBRASKA on 08/06/2016 06:34:59.

Introduction

Highly symmetrical chiral macrocycles are of broad interest due to their applications as molecular building blocks, chiral catalysts and chiral discriminating agents. The widely used methodology for facile synthesis of macrocycles is based on thermodynamically controlled imination reactions of dialdehydes with diamines. The subsequent reduction of readily formed polyimine macrocycles of regular structure provide chemically more stable and functionally feasible polyamines.[1–3] In the [3 + 3] cyclocondensation reaction between equimolar amounts of both: a dialdehyde and a diamine, triangular products are the most readily formed. The first reported successful, quantitative synthesis of triangular hexaimine (trianglimine) and its reduction product (trianglamine) received a wide attention as a convenient method for construction of chiral, symmetrical aza-macrocycles.[4–7] There are a few factors, which contribute to favoring macrocyclization over acyclic polycondensation. First, the symmetrical cyclic structure of the product is controlled in the thermodynamically driven reversible imination step. Second, the substrates should have limited flexibility, restricting the number of conformers accessible at the reaction temperature. Third, the macrocycle chirality originates from the use of enantiomerically pure diamine substrate of C_2 symmetry usually. From the library of diamines, the most frequently used chiral scaffold for synthesis of shape-persistent macrocycles is the enantiomerically pure *trans*-1,2-diaminecyclohexane (DACH, **1**).[8] Among aromatic dialdehydes, the terephthalaldehyde and its derivatives having linear formyl groups arrangement are ideally geometrically predisposed to provide trianglimines.

Structural modification of the trianglimine could be done at the pre-macrocyclisation stage only, with the use of modified substrates, usually dialdehydes. Analysis of literature precedents led to conclusion, that the use of structurally modified 1,4-dialdehydes in synthesis provided mainly symmetrical products, even when the aldehyde was non-symmetrical.[9] The

[a]*Department of Chemistry, Adam Mickiewicz University, Umultowska 89B, 61 614 Poznan, Poland. E-mail: gajewy@amu.edu.pl; marcin.kwit@amu.edu.pl*

[b]*Wielkopolska Center for Advanced Technologies (WCAT), Umultowska 89C, 61 614 Poznan, Poland*

† Dedicated to Prof. Janusz Jurczak on the occasion of his 75 birthday.

‡ Electronic supplementary information (ESI) available: Experimental procedures, calculation details, copies of NMR, MS and IR spectra, Fig. SI_1–SI_55, tabulated total and relative energies for calculated structures, Cartesian coordinates, conditions and retention times for HPLC separation of enantiomers, literature references for the products of asymmetric hydrosilylation of ketones. See DOI: 10.1039/c6ra06095a

This journal is © The Royal Society of Chemistry 2016

Published on 27 May 2016. Downloaded by UNIVERSITY OF NEBRASKA on 08/06/2016 06:34:59.

decisive factor responsible for the preference of symmetrical (thermodynamic) over non-symmetrical (kinetic) product of reversible reactions with the same bond formation enthalpies is ascribed to so called "entropy of symmetry".[10–12] According to this rule, among several possible products, the one with the highest symmetry is characterized by the lowest relative energy.

While the parent trianglimines have only limited applications due to instability of C=N double bond,[13] their reduced congeners were applied as chiral discriminating agents, ligands and organocatalysts.[14–16] Recently Tanaka *et al.*, reported gelation properties of trianglimine containing azobenzene chromophore. The macrocycle is characterized by rather complex structural behavior determined by the presence of –N=N– group. The gel is formed upon cooling of the benzene solution of the macrocycle and after photoirradiation by UV light (300–400 nm) for several hours is transformed to sol. The original gel was recovered upon heating.[13]

The [Zn–diamine]-catalyzed enantioselective hydrosilylation of prochiral ketones is a practical and convenient synthetic method providing optically active alcohols *via* reduction of the carbon–oxygen double bond. A typical catalyst system is formed *in situ* from equimolar amounts of dialkyl zinc and a secondary diamine and reduction proceeds smoothly without using hydrogen gas.[17–19] Recently reported chiral tetra- and hexamine macrocycles derived from DACH, in complexes with diethylzinc efficiently catalyze asymmetric hydrosilylation of ketones and imines with enantiomeric excess of the product up to 89% and >99%, respectively for alcohols and amines.[20,21]

Continuing our interest in macrocyclic compounds capable of serving certain functions, we decided to synthesize chiral triangular macrocycles containing functionalities of the contrasting character. Our goal was not the multiplication of new compounds but rather in depth study of the structure, properties and applications of relatively simple exemplary trianglimines. Structure of the polyimine compounds were studied by means of experimental/theoretical approach, with particular emphasis on circular dichroism spectroscopy. We expected the decisive role of substituents, attached to aromatic rings, for tuning of molecular/supramolecular properties of the trianglimines and trianglamines. Despite recent progress,[22] the Zn-catalyzed asymmetric reduction is still relatively unexplored, thus we applied the reduced macrocycles, previously obtained at cycloimination stage, in asymmetric hydrosilylation of ketones.

Results and discussion

Materials and methods

From virtually unlimited number of the terephthaldehyde derivatives we chose representative ones having either methoxy or nitro groups. 2,5-Dimethoxyterepthaldehyde (**2**) was obtained according to the procedure previously reported by Kuhnert *et al.*, starting from 1,4-dimethoxybenzene.[23] 2-Nitroterephthalaldehyde (**3**) was obtained after reduction of 2-nitroterephthalic acid with diborane followed by PCC-oxidation of corresponding diol intermediate.[24] 2-Methoxyterepthaldehyde (**4**) was obtained from 2,5-dimethylanisole in sequence of reactions. At the first stage, 2,5-dimethylanisole was oxidized to 2-methoxyterepthalic acid.[25] Then, the acid was reduced with diborane to the corresponding diol which was further PCC-oxidized to the aldehyde **4**. Despite many attempts we were unsuccessful to synthesize 2,5-dinitroterephthaldehyde.

The trianglimine macrocycles **5–7** were obtained *via* cyclocondensation reactions between equimolar amounts of **1** and corresponding aldehyde **2–4** in dichloromethane solution. The mixtures were stirred for 24 hours and after evaporation to dryness, the crude products **5–7** were obtained quantitatively. The recorded ^{1}H NMR and FT-IR spectra showed completely disappearance of respective aldehyde signals while mass spectrometry confirmed [3 + 3] reaction stoichiometry. Subsequent reductions of the trianglimines **5** and **6** with $NaBH_4$ in dichloromethane–methanol mixture provide trianglamines **8** and **9** with almost quantitative yields (Scheme 1). The trianglamines **8** and **9** were used as zinc ligands for asymmetric hydrosilylation of selected prochiral ketones. Due to the formation of non-separable mixture of [3 + 3] products differ in symmetry (*vide infra*), the trianglimine **7** was not reduced.

Detailed experimental procedures and full spectroscopic characterization for all compounds were deposited in ESI.‡

The UV and ECD spectra of trianglimines were measured in chloroform. The gelation properties of trianglimine **6** were studied using solvents of different polarity and at various concentrations of the gelator. ECD spectra of gels were measured using demountable quartz cell with path length of 0.01 cm. VCD spectra of **6** were measured in deuteriochloroform solution of concentration 20 mg per 0.15 mL, using BaF_2 cell with 25 μm path length.

To rationalize the experimental observations we performed quantum-chemical calculations at the DFT level with the use of B3LYP hybrid functional. The possible structures that include both constitutional and conformational isomers of the imine macrocycles as well as some model compounds were pre-optimized at the molecular mechanic level (MM3 force field as implemented in Scigress software).[26] Then, all structures found at this stage were optimized at the B3LYP/6-31(d) level and re-optimized with the use of the same hybrid functional and enhanced triple-ζ basis set, 6-311G(d,p). To estimate solvent influence on the structure and energy of the species under study, the IEFPCM solvent model of chloroform was employed.[27] The structures thus obtained were the real minimum energy isomers. The total and free energy values were used to obtain the Boltzmann population at 298.15 K.

For CD calculations only the real minimum energy conformers that differed from the most stable one by less than 2 kcal mol^{-1} were taken into consideration.[28] Rotatory strengths were calculated employing CAM-B3LYP,[29] M06-2X,[30] B2LYP[31] and LC-wPBE[32] hybrid functionals, all in conjunction with 6-311++G(d,p) basis set and IEFPCM solvent model.[27] Such an approach was successfully employed for us to study large systems of high structural diversity.[33] Since all the TD-DFT methods gave very similar results only these obtained with the use of IEFPCM/TD-CAM-B3LYP/6-311++G(d,p) method were discussed here. The rotatory strengths were calculated using both length and velocity representations. Due to the negligible

Published on 27 May 2016. Downloaded by UNIVERSITY OF NEBRASKA on 08/06/2016 06:34:59.

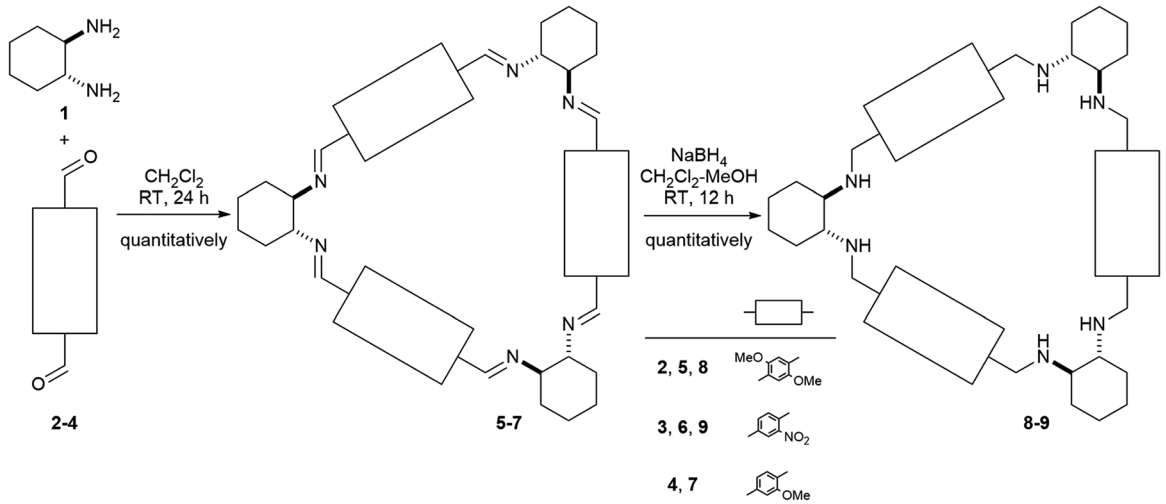

Scheme 1 Synthesis of trianglimines **5–7** and trianglamines **8** and **9** from **1** and aldehydes **2–4**.

differences between the length and velocity calculated values, only the velocity representations were used in the present study. The ECD and VCD spectra were simulated by overlapping Gaussian or Lorenzian functions for each transition.[34,35] For the remaining results and detailed calculation procedure see Theoretical section in ESI.‡

Structure

As a result of syntheses, we expected highly symmetrical products **5–7**, in accordance with the previously mentioned entropy of symmetry rule. Experimentally, the preference for the formation of symmetrical over non-symmetrical product is revealed in the reduced number of signals in the ^{1}H and ^{13}C NMR spectra, corresponding to a symmetry of given macrocycle. For molecular structures generated *in silico* the more symmetrical macrocycle should have lower relative energy than less-symmetrical one(s).

For **5** only one C<u>H</u>N and one C<u>H</u>$_{Ar}$ signals are observed in ^{1}H NMR spectrum (Fig. 1a), in agreement with postulated D_3 symmetry of the molecule. From the two possible D_3-symmetrical isomers, the one characterized by *anti* orientation of methoxy groups and the nearest neighboring nitrogen imine atoms is lower in energy by over 23 kcal mol^{-1} (see Fig. 1a and SI_1–SI_2 and Table SI_1 in ESI‡), than isomer of *syn* arrangements of MeO and C=N fragments, in agreement with previously reported data.[23] The methoxy groups in **5** are oriented perpendicular to the mean macrocycle plane and situated in between imine and aromatic hydrogen atoms, whereas for the higher-energy isomer electrostatic repulsion between oxygen and nitrogen atoms in close proximity caused significant increase of energy.

The case of **6** is more complex. The ^{1}H as well as ^{13}C NMR spectra of **6** showed more signals than it was expected for the C_3-symmetrical molecule. In aromatic region of ^{13}C NMR spectrum of **6** there are 24 signals of respective carbon atoms, which suggested the trivial C_1 symmetry of the whole macrocycle. The ^{1}H NMR spectrum alone is difficult to interpretation due to fractional integration of signals, however, we can distinguish four set of signals appeared at spectral ranges 8–59–8.35 (**a**), 8.21–8.17 (**b**), 7.99–7.82 (**c**) and 7.56–7.48 (**d**) ppm. A

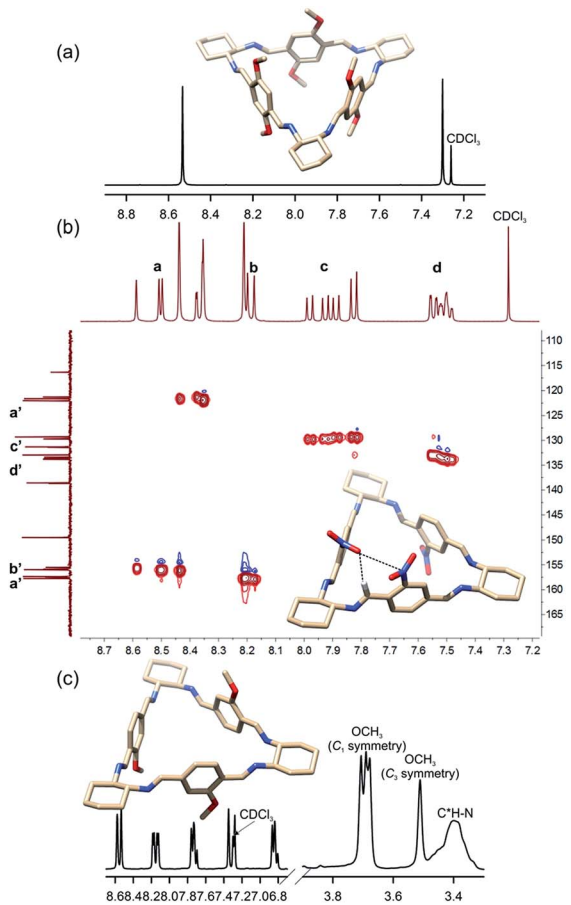

Fig. 1 Diagnostic aromatic region of the ^{1}H NMR spectrum of **5** (a), the aromatic part of the HSQC spectrum of **6** (b) and the diagnostic regions of the ^{1}H NMR spectrum of **7** (c). Insert shows the lowest-energy calculated structure of **5–7**, the latest two characterized by C_1 symmetry (some hydrogen atoms were omitted for clarity). Dashed lines indicate possible attractive interactions.

 This journal is © The Royal Society of Chemistry 2016

Published on 27 May 2016. Downloaded by UNIVERSITY OF NEBRASKA on 08/06/2016 06:34:59.

HSQC spectrum of **6** (Fig. 1b) allowed correlation between respective signals and indicates that the ^{1}H NMR signals **a**, **b** correlate with the six signals of the imine carbon atoms **a′**, whereas the ^{1}H NMR signals **c** and **d** correlate with nine signals of tertiary aromatic carbon atoms **b′**. The number of signals did not change during variable temperature (within −60 to +50 °C range) NMR experiments that exclude conformational isomerism (see ESI, Fig. SI_39‡).

After reduction of **6** to amine **9**, the **a**, **b** proton signals disappeared whereas **c**, **d** remains in almost the same spectral region. Observed in ^{1}H NMR spectrum of **9** signals that appeared at $\delta = 7.93$ and 7.89 as set of two singlets matched to protons in *ortho* position to both nitro and imino groups. Measured integration of these signals is 2 to 1, in excellent agreement with C_1 symmetry of hexaamine and its parent hexaimine macrocycle **6**.

Generated "*in silico*" the lowest-energy structure of **6** is characterized by the highest allowed C_3 symmetry. At each side of the triangle the nitro group and the nearest neighboring imine nitrogen atom are in *anti* conformation. The theoretical results prove the entropy of symmetry rule, however they are inconsistent with the experimental data. The predicted for the C_3-symmetrical structure downfield region of ^{1}H NMR spectrum should consist of 3 signals of aromatic protons (singlet and two doublets) and two singlets originated from CHN methine protons. The NMR spectra confirmed formation of the non-symmetrical product (*vide supra*). Disregarding C_3-symmetrical isomers, not-formed in the reaction, the most preferable (on the basis on DFT results) the C_1-symmetrical isomer of **6**, shown in Fig. 1b (see also Fig. SI_3 and Table SI_1 in ESI‡), is characterized by *anti*, *anti*, *syn* conformation of nitro groups related to respective neighboring imine nitrogen atoms. In this particular conformation, there are possible attractive interactions involved negatively charged oxygen atom of one nitro group (in *syn* conformation) and both the imine hydrogen atom and the positively charged nitrogen atom from the neighboring nitro group in *anti* conformation.

The noted discrepancy between experiment and the entropy of symmetry rule may originate in preference to form kinetic over thermodynamic macrocyclic product **6**. Thereby, the macrocycle structure is determined by the structure of intermediates appeared during cycloimination reaction.

We decided to look deeper into mechanism of the macrocycle **6** formation using ^{1}H NMR and ESI-TOF MS measurements, supported by DFT calculations (Fig. 2 and ESI‡).[36] The test reaction between equimolar amounts of **1** and **3** was conducted in NMR tube in $CDCl_3$ at concentration of 0.1 M, the liberated water was not removed and a content of the test tube was protected against the influence of external environment. The same conditions were used for parallel reaction conducted in DCM. For MS measurements, the aliquot of the reaction mixture was diluted by methanol to a concentration of 0.1 mM and directly injected.

The cycloimination reaction started immediately after mixing of substrates. The ^{1}H NMR spectra showed gradual change in the region of the aromatic proton absorption as well as between 4 and 3 ppm. The completely disappearance of the aldehyde CHO signals and formation of **6** as the sole product was observed within 7 hours. The prolongation of the reaction time to 60 hours or gentle heating of the reaction mixture did not alter the shape nor the number of signals observed in ^{1}H NMR spectrum.

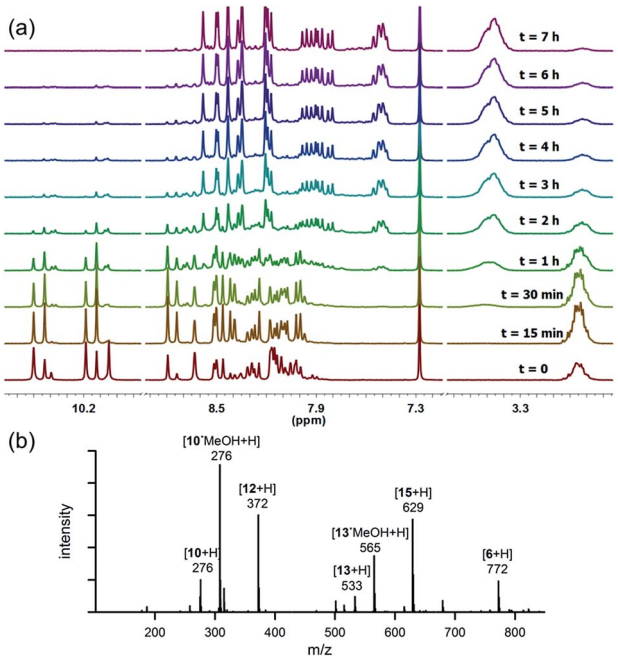

Fig. 2 Parts of the ^{1}H NMR spectra measured at the time intervals for the reaction between **1** and **3** (a) and exemplary ESI-TOF mass spectra recorded after 1 hour from the start of the reaction (b).

The ESI-TOF MS measurements run parallel to NMR experiments allowed to identify main reaction intermediates and to propose the mechanism of formation the trianglimine **6** (Scheme 2). In an exemplary MS spectrum recorded after 1 hour from the reaction start, the highest intensity peak of $m/z = 308$ corresponds to protonated [1 + 1] intermediate **10** which condenses with another DACH molecule to form [1 + 2] product **12**. Surprisingly, the [2 + 1] product **11** of $m/z = 437$ (M + H) was not detected, probably due to rapid interconversion into [2 + 2] intermediate **13**. Similarly, the [3 + 2] intermediate **14** and open chain pentaimine **16** were not detected, which suggested very fast process of macrocycle ring closing. Alternatively, triimine **13** may be formed by subsequent condensation of **10** with **1** and then with aldehyde **3**.

DFT calculations performed for intermediates **10** and **15** shed a light on the stereochemical course of this particular macrocyclisation reaction. From the two possible monoimines **10a** and **10b**, differ in the position of the nitro substituent with respect to the imine group, the one having NO_2 group in *ortho* position is energetically preferred by *ca.* 1.3 kcal mol^{-1}. The tetraimine species **15a–15c** are the most important intermediates since their structure determine the whole structure of the macrocycle. Symmetrical intermediate always provide the non-symmetrical macrocycle, whereas from non-symmetrical one may form either symmetrical or non-symmetrical product **6**. From isomers **15a–15c**, the C_2-symmetrical ones **15a** and **15c**

Published on 27 May 2016. Downloaded by UNIVERSITY OF NEBRASKA on 08/06/2016 06:34:59.

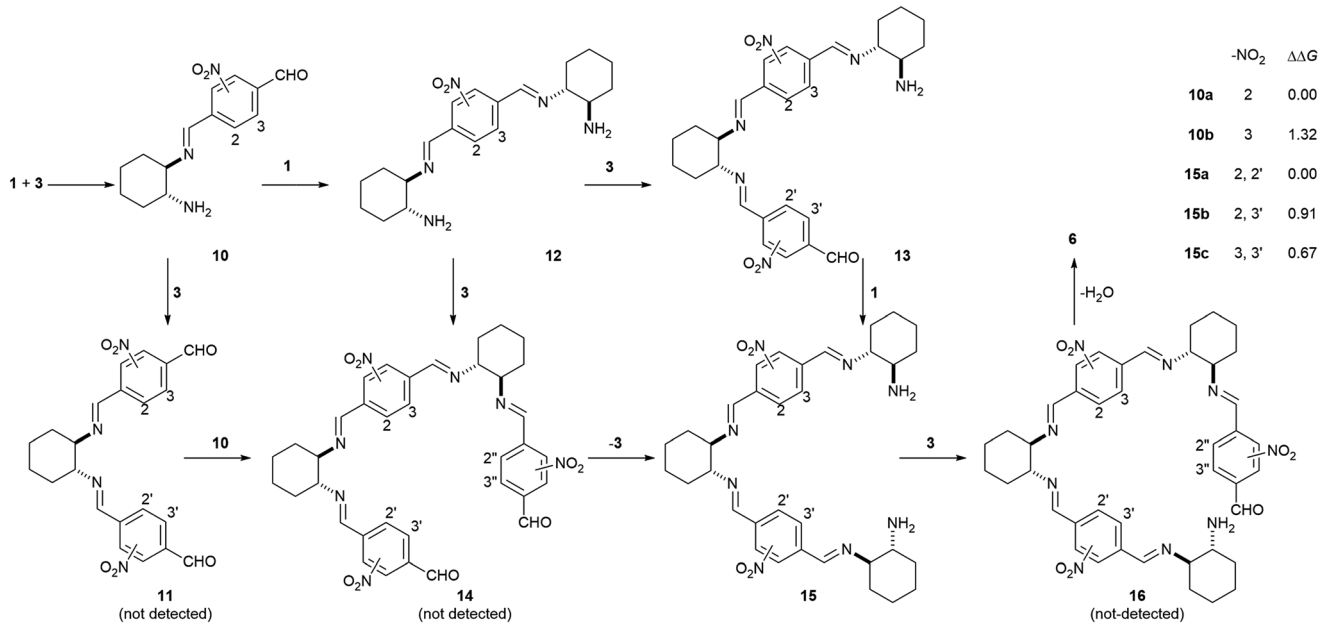

Scheme 2 Stepwise [3 + 3] cycloimination reaction between **1** and **3** (due to the clarity of presentation only a few from all possible sub-paths of the reaction were shown). The values in the upper right corner indicate calculated relative free energies ($\Delta\Delta G$, in kcal mol^{-1}) between respective isomers differ in the NO_2 group location (within each set of constitutional isomers only the lowest-energy conformers were considered here, see also ESI‡ for the remaining results).

covered almost 90% of energetically allowed structures responsible for further formation of non-symmetrical macrocycle **6**.

Similar to the above-mentioned example, in ^{1}H (shown in Fig. 1c) as well as in ^{13}C NMR spectrum of **7** more signals were observed than expected for C_3 symmetry. The number and the shape of the diagnostic OCH_3 signals (observed in ^{1}H and ^{13}C NMR spectra) suggested the formation of equilibrium mixture of non-symmetrical and symmetrical macrocycles. Estimated integration of the OCH_3 signals is 70 to 30, in favor of the C_1-symmetrical macrocycle.

The ^{1}H NMR spectra measured at the time intervals for the reaction between **1** and **4** showed gradual disappearance of C<u>H</u>O signals. The reaction is completed within 1.5 hour and an established equilibrium between C_3- and C_1-symmetrical isomers did not change even if the reaction was prolongated to one week.

From all possible calculated isomers, there are two characterized by all-*anti* orientation of methoxy groups and the nearest neighboring nitrogen imine atoms. The C_1-symmetrical structure is lower in energy by 1 kcal mol^{-1} than the higher symmetrical one. The calculated $\Delta\Delta G$ energy difference corresponds to 85% abundance of the C_1-symmetrical structure in the mixture, in very good agreement with the experimental data (see Fig. 1c and SI_4 and Table SI_1 in ESI‡). The preference for C_1-symmetrical, all-*anti*-**7** is due to the minimization of O···N and O···O electrostatic interactions.

Note, even one *syn* arrangement of OCH_3 and C=N groups within macrocycle structure caused in significant energy increase.

The "*in silico*" estimated mechanism of the macrocycle **7** formation suggested dominant role of non-symmetrical intermediates over the symmetrical ones (Fig. SI_7–SI_10 and Table SI_10, ESI‡). However, the domination of non-symmetrical intermediates is not reflected in preferred formation of symmetrical macrocycle (*vide supra*). Thus, formation of non-symmetrical macrocycle is energetically privileged indeed. However, it remains in contradiction with the entropy of symmetry rule.

The main difference between respective structures of intermediates, provide either **6** or **7**, is due to the role of substituent. The nitro groups are involved in intramolecular hydrogen bonding that strongly stabilize the structure. Contrary, the methoxy groups control the structure by electrostatic and to less extend by sterical interactions.

Chiroptical properties

ECD spectra of 5 and 6. The measured in chloroform solution and calculated at the TD-DFT level UV and ECD spectra of the macrocycles **5–6** are shown in Fig. 3a.

The presence of aromatic chromophores within macrocycle caused generation of strong exciton-type Cotton effects in ECD spectra that correspond to the UV absorption maxima allowing interpretation of the experimental results on the basis of empirical exciton chirality rule.[37] In the UV spectrum of **5** two absorption maxima at around 361 and 276 nm appeared. The TD-DFT calculations, performed for model "isolated" single chromophore, indicated that the low-energy electronic transition involves HOMO and LUMO orbitals, whereas the higher energy transition involves HOMO-1 and LUMO orbitals. These absorption maxima associated with two sets of bisignate exciton Cotton effects that may be correlated with molecular chirality.

 This journal is © The Royal Society of Chemistry 2016

Published on 27 May 2016. Downloaded by UNIVERSITY OF NEBRASKA on 08/06/2016 06:34:59.

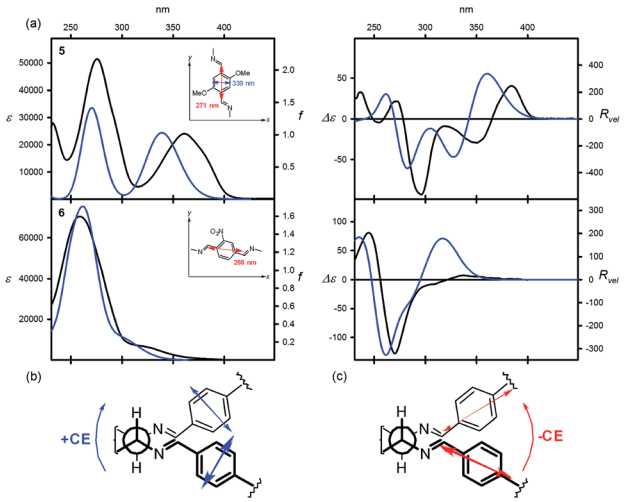

Fig. 3 UV (left panel) and ECD (right panel) spectra of **5** and **6**, measured (black lines) in chloroform solution and calculated (blue lines) at the IEFPCM/CAM-B3LYP/6-311++G(d,p) level (a). The calculated spectra were not wavelength corrected. Inserts shows polarization of the electronic transition moments of the highest oscillator strength. The Newman projections along the C*–C* bond in cyclohexane moiety explain the origin of the long-wavelength positive exciton couplet for **5** (b) and negative short-wavelength exciton couplets (c) for **5** and **6** (functional groups were omitted for clarity).

The positive sign of the long-wavelength couplet originated from interacting electronic transition dipole moments polarized parallel to the line connected oxygen atoms in the chromophore (perpendicular to the long axis of the chromophore and mean macrocycle plane). The sign of the low-energy couplet remains in disagreement with the negative diamine chirality (see Fig. 3b).[38] The second, higher-energy negative exciton couplet, appeared at around 270 nm, is in agreement with negative sign of N–C*–C*–N torsion angle and originates from interactions between electronic transition dipole moments polarized along the long axis of the chromophore (see Fig. 3c).

The UV spectrum of **6** is characterized by strong absorption maximum appeared at 259 nm. The electronic transition dipole moments of the highest oscillator strength, polarized along the long axis of the chromophore, generated negative exciton couplet centered at around 250 nm. Contrary to **5**, the electronic transitions polarized perpendicular to the long axis of the chromophore did not affect the experimental ECD spectrum of **6**.

The above empirical analyses remain in excellent agreement with the results of TD-DFT calculations. For macrocycle **5** the experimental/theoretical approach to the analysis of ECD spectra allowed to distinguish between *syn* and *anti* isomers. ECD spectrum calculated for the higher-energy *syn* isomer exhibits negative long-wavelength exciton couplet, in disagreement with experimental data.

For **6** the overestimated intensity of the long-wavelength positive Cotton effects in comparison to the experimental one is the results of the "static", frozen geometry of the macrocycle. This particular Cotton effects is associated with the electronic transition polarized almost perpendicularly to the long axis of the chromophore and involved HOMO-3, HOMO-5 and LUMO orbitals. In the real molecule, rotation of the chromophore around C–C bonds is fast and caused almost complete cancelation of the generated Cotton effects.

It is worth noting, that the overall shape of experimental UV and ECD spectra of **7** (shown on Fig. SI_12, ESI‡) are very close to these measured for trianglimine **5**. However, the presence of only one methoxy group in each aromatic arm of the triangle caused blue shift of respective UV and ECD maxima. The UV absorption bands that correspond to two exciton couplets observed in ECD spectrum appeared at 328 and 273 nm. The positive long-wavelength couplet appeared at around 320 nm is due to the interactions between electronic transition dipole moments, polarized almost perpendicular to the long axis of the chromophore. Similarly to trianglimines **5** and **6**, the second negative exciton couplet (at around 270 nm) originated from interactions between electronic transitions dipole moments polarized along the long axis of the chromophore.

Changes in ECD spectra of 5 upon protonation. Different substitution patterns were responsible for contrasting behavior of the **5** and **6** observed upon protonation. Acidification of the chloroform solution of **6** by methanesulfonic acid caused the significant decreasing of the intensity of both UV and ECD absorption maxima, due to the decomposition of the macrocycle. The hexaimine **5** is an exception. Gradual titrations of **5** by methanesulfonic acid solution revealed in strong bathochromic shift of the long-wavelength absorption maximum (see Fig. SI_14 and SI_15‡). Just one equivalent of the acid caused appearance of the new absorption band at around 427 nm. Addition of more than three equivalents of the acid shifted this band by further *ca.* 30 nm into low-energy region of the spectrum. Addition of more than 6 equivalents of the acid did not alter shape of the spectrum. The same situation is observed in ECD spectra (see Fig. 4). The first long-wavelength Cotton effect was red-shifted by 140 nm from 384 to 522 nm retaining its intensity regardless the amount of the acid added. The second most intense UV absorption band remains not altered by acidification. The negative Cotton effect associated with this band did not shift, however, its intensity increased over two-fold for fully protonated macrocycle in comparison with the non-protonated one.

The same behavior is observed for molecules "*in silico*". TD-DFT calculations performed for optimized structures of non-protonated, mono-, di-, tri-, tetra-, penta- and hexaprotonated **5** perfectly reflected the experiment.

Note, that UV and ECD spectra measured during titration of **7** by methanesulfonic acid showed similar changes to those seen during the titration of **5** (see Fig. SI_26 and SI_27, ESI‡).

Experimental and calculated VCD spectra of 6. Our analysis of the trianglimine **6** chiroptical properties was extended on vibrational spectroscopy. The experimental IR and VCD spectra were measured in deuterated chloroform. The DFT calculations were carried out using the same level of theory as it was used for the geometry optimization of all isomers of **6**. The experimental and calculated for the lowest-energy C_1-symmetrical isomer of **6** spectra are shown in Fig. 5.

As can be seen, the calculated and experimental spectra are in reasonable agreement. Surprisingly, the region of strong

Published on 27 May 2016. Downloaded by UNIVERSITY OF NEBRASKA on 08/06/2016 06:34:59.

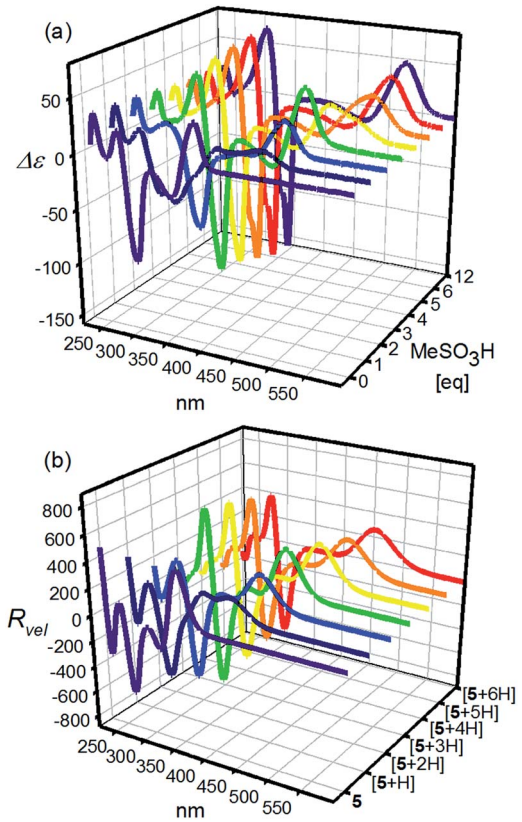

Fig. 4 ECD spectra measured during titration of **5** by methanesulfonic acid (a) and calculated at the IEFPCM/TD-CAM-B3LYP/6-311++G(d,p) level for non-protonated, mono-, di-, tri-, tetra-, penta- and hexaprotonated **5**, optimized at the IEFPCM/B3LYP/6-311G(d,p) level (b). Wavelengths were not corrected.

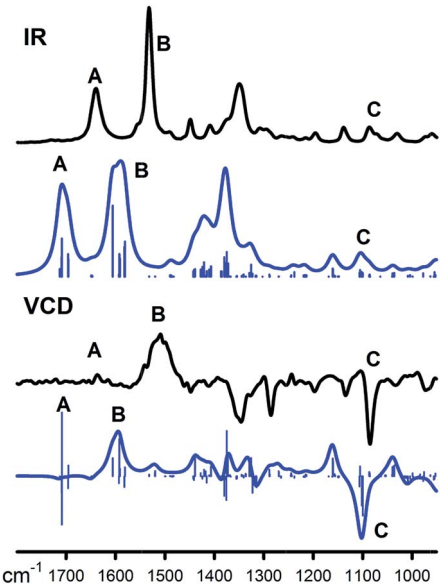

Fig. 5 IR (top) and VCD (bottom) spectra of **6** measured in $CDCl_3$ (black lines) and calculated at the IEFPCM/B3LYP/6-311G(d,p) level of theory (blue lines). Vertical bars represent calculated dipole and rotatory strengths. Calculated frequencies were not scaled.

N=C absorption at around 1640 cm^{-1} (denoted here as **A**) is less convenient for analysis of VCD intensities. The observed in this region Cotton effects are very weak due to the almost total cancelation of rotatory strengths of opposite signs but equal intensities. The peak in IR spectrum appeared at around 1530 cm^{-1} (**B**) that corresponds to positive Cotton effect in VCD spectrum is associated with N–O asymmetric stretch. The observed broadening of the VCD signal is apparently due to the C_1 macrocycle symmetry and overlapping of rotatory strengths originated from non-equivalent nitro groups. The characteristic strong negative Cotton effect appeared at 1080 cm^{-1} (**C**) is generated by rotatory strengths originated mostly from C–H bending and in IR spectrum is associated with peak of small intensity. Note, the region of aliphatic C–H bending modes in VCD spectrum is not well reproduced by calculations and thereby difficult to interpretation.

Gelation properties

Trying to grow a single crystal suitable for X-ray diffraction analysis unexpectedly, a gel was obtained when **6** (15 mg) was dissolved in chloroform (0.1 mL) and the resulted solution was diluted with an absolute ethanol at room temperature. The gel thus obtained was translucent, slightly yellow colored and stable at room temperature in closed container for a few weeks. However, the mechanical mixing of the gel destructed its structure. The minimum gelation concentration determined through a series of dilution experiments is as low as 4.8 mg mL^{-1} (6.3×10^{-3} M, 0.5% w/v) for the mixture composed of 1 part (vol.) of $CHCl_3$ and 30 parts (vol.) of ethanol (Fig. 6a). We established that this gelation occurs also for the chloroform solution of **6** mixed with an excess of other solvent, such as alcohols, whereas non-polar solvents: hexane, toluene and diethyl ether do not form a gel (see Table 1). From the protic solvent tested, differing in the length and structure of an alkyl chain, the linear alcohols gelated better. However, the elongation of the chain above 3 carbon atoms has reverse effect. While *n*-propanol forms a gel, the use of *n*-butanol and its isomers at best lead to a partial gelation. On the other hand, the methanolic solution of **6**, at concentration below 4.8 mg mL^{-1}, does not gelate. Note, pre-dissolving of **6** in chloroform is compulsory due to poor or even insolubility of the macrocycle in common non-chlorinated organic solvents. The probable gelation mechanism in ethanol is the formation of the cascades of hydrogen bonds involving macrocycle's nitro and solvent's hydroxy groups.

The gel made from **6** was dried and analyzed by scanning electron microscopy (SEM) to obtain visual insights into the molecular aggregate. The SEM photographs was shown in Fig. 6b and exhibited the presence of irregular, rounded structures having lateral dimensions of a few microns and the height of the order of tens/hundreds of nm. The material form amorphous phase, as revealed by PXRD analysis. On an AFM image of 500 nm × 500 nm scale is visible porous structure of the material.

Similar tests performed with **5**, **7** as well as for the triangl-amines **8** and **9** did not lead to gelation in any case. Surprisingly,

 This journal is © The Royal Society of Chemistry 2016

Published on 27 May 2016. Downloaded by UNIVERSITY OF NEBRASKA on 08/06/2016 06:34:59.

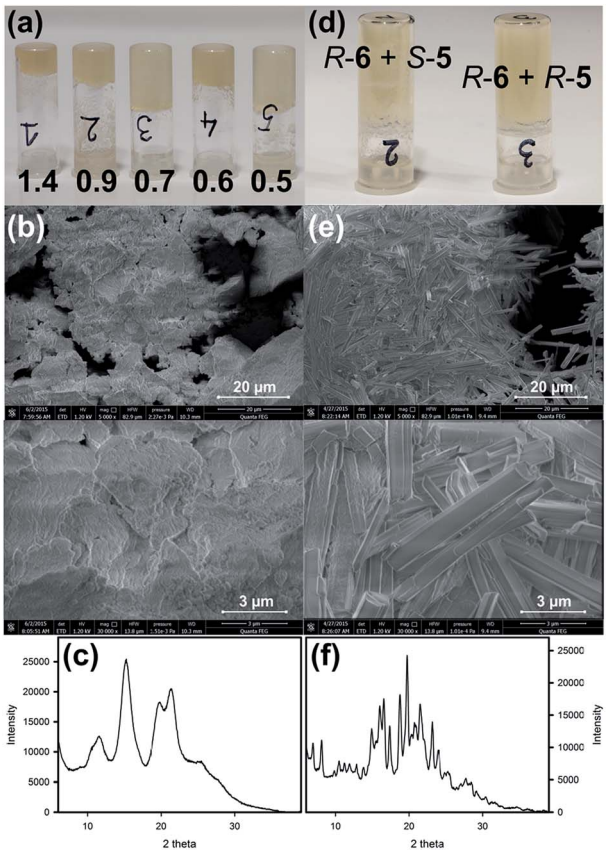

Fig. 6 Macrocycle **6** gels made from samples of different concentrations (w/v) (a). SEM images of macrocycle **6** gel (b) and X-ray diffraction pattern of the quickly dried gel sample (c). Gels made from macrocycle **6** doped with all-(*S*)-**5** and all-(*R*)-**5** (d). SEM images of macrocycle **6** gel doped with all-(*R*)-**5** (e) and X-ray diffraction pattern of the quickly dried gel sample (f).

the chloroform solution of **6** that contains the same weighting amount of guest trianglimine **5** shows the same gelation abilities (Fig. 6d). The concentration of each component **5** and **6** was 0.45% w/v and gels were formed after diluting by absolute ethanol, irrespective to chirality of **5**. The gels were opaque and after drying, were analyzed by SEM and AFM techniques. Both gels, differ in absolute configuration of the guest, are characterized by the same microcrystalline morphology. The height of the crystal is approx. 650 nm and the microcrystals may be characterized as "twins" where each part of the crystal is characterized by *ca.* 300 nm heights. The crystalline phase of the mixed gels was confirmed by PXRD measurements. Unfortunately, despite many attempts we were not able to obtain a single crystal from the mixture containing **5** and **6**.

As the materials obtained were chiral we decided to measure their ECD spectra and confronted them with the ECD spectra measured for a given compound in chloroform solution (see Fig. 7).

In ECD spectrum measured for gel made from **6** significantly enhanced long-wavelength positive Cotton effect is observed. As we mentioned above this particular Cotton effect is generated by interacting electronic transition dipole moments polarized

Table 1 Gelation studies of **6** in various solvent mixtures

Run	Additive[a]	Concentration (mg mL^{-1})	Observation[b]
1	EtOH	13.6	G
2	EtOH	9.4	G
3	EtOH	7.1	G
4	EtOH	5.8	G
5	EtOH	4.8	G
6	EtOH	3.7	PG
7	MeOH	5.8	G
8	MeOH	4.8	PG
9	*n*-PrOH	5.8	G
10	*i*-PrOH	5.8	PG
11	*n*-BuOH	5.8	PG
12	*sec*-BuOH	5.8	PG
13	*tert*-BuOH	5.8	S
14	DMF	5.8	S
15	DMSO	5.8	S
16	MeCN	5.8	PG
17	Toluene	5.8	S
18	AcOEt	5.8	S

[a] All tests were performed using a constant amount of **5** (15 mg) in 0.1 mL of chloroform that was diluted by the second solvent. [b] G = gelation, PG = partial gelation, S = solution.

perpendicularly to the long axis of the chromophore and canceled upon free rotation of the aryl part. As it was supposed, gelation may proceed through hydrogen bonding formation between the gelator and the solvent. Thus, the formation of ordered superstructure may cause hindered internal rotation of the aryl fragments around C–C bonds, thereby increase intensity of the long-wavelength Cotton effect. The ECD spectrum measured for gel containing all-(*R*)-**6** and all-(*R*)-**5** is strongly affected by Cotton effects originated from the dopand. This revealed in similar shape of the ECD spectrum measured for gel and for solution of all-(*R*)-**5**. Contrary, in the same spectral region the ECD spectrum measured for gel made from heterochiral **5** and **6** exhibited Cotton effect of the opposite sign,

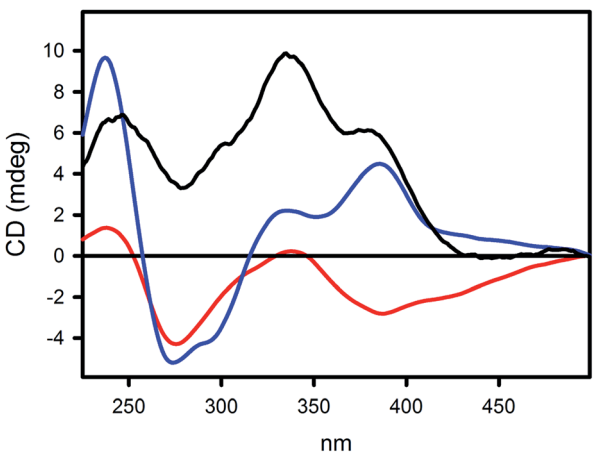

Fig. 7 ECD spectra of gels made from all-(*R*)-**6** (black line), mixture of all-(*R*)-**6** and all-(*R*)-**5** (blue line) and mixture of all-(*R*)-**6** and all-(*S*)-**5** (red line).

Published on 27 May 2016. Downloaded by UNIVERSITY OF NEBRASKA on 08/06/2016 06:34:59.

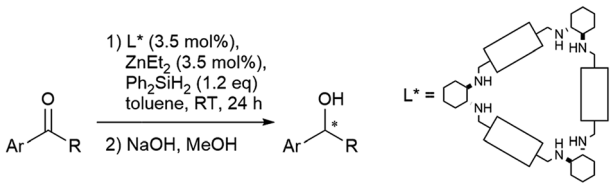

Scheme 3 Zinc–trianglamine-catalyzed asymmetric hydrosilylation of prochiral ketones.

which suggested less influence of the dopand on overall chiroptical properties of the sample. In the higher energy region (below 350 nm), both spectra are similar in the sequence of the Cotton effects (positive/negative/positive). However, the intensities of the respective Cotton effects are quite different and for heterochiral gel is almost two-fold higher. The observed Cotton effects are superposition of the intra- or intermolecular interactions, however, the definitely distinguish between the two effects is not possible at the moment.

Zn–trianglamine catalyzed asymmetric hydrosilylation of prochiral ketones

Finally, we attempted to use the obtained trianglamines **8** and **9** as zinc ligands in the asymmetric hydrosilylation (AHS) of various prochiral ketones (Scheme 3). The catalytically active species were generated *in situ* by mixing of equimolar amounts of diethyl zinc with respective ligand. The catalyst loading was 3.5 mol% in all cases, since the lower amounts caused significant decrease of asymmetric induction level. As the reducing agent, we used diphenylsilane and all reactions were carried out for 24 h at room temperature in dry and degassed toluene. As the test reaction we choose AHS of 4-methyacetophenone.

The initial examination of the effect of the ligand structure on the yield and enantioselectivity of the test reaction provided very promising results in terms of enantioselectivity compared to that previously published by others and us (Table 2).[20,22,39] The best results were obtained when the methoxy-substituted trianglamine **8** was employed as ligand (Table 2, entry 1). With the use of **8** the asymmetric induction reached 98% with completely conversion of the substrate. To our best knowledge, this is the best results obtained so far for zinc–diamine-based catalytic systems. The trianglamine **9** gave product with good asymmetric induction and conversion, however, these results were not better to that obtained with the use of **8** and comparable to the results obtained when non-modified trianglamine was employed as the zinc ligand (Table 2, entry 2).

Having established **8** and **9** as suitable ligands for asymmetric hydrosilylation a selected alkyl–aryl and aryl–aryl prochiral ketones were reduced in above mentioned conditions (3.5 mol% of catalyst, 1.2 equiv. of silane in toluene). The results are summarized in Table 2. In general, the use of **8** and **9** as ligands provided products of the higher asymmetric induction levels than those obtained with other trianglamines.[20] On the other hand, the increased enantioselectivity is with expense of the isolated yield of the product, and the higher chemical yield did not exceed 65%. Good results in term of enantioselectivity were obtained for the products significantly differ in the size of substituents (for example, phenyl *vs.* cyclohexyl, Table 2, entries 5 and 6). The prochiral substrates of benzophenone-type gave moderate levels of asymmetric inductions (Table 2, entries 13–18) due to low stereo-difference between substituents of the carbonyl group. The most problematic aryl-trifluoromethyl ketones were reduced with the very low level of asymmetric induction (Table 2, entries 19–21), regardless the size of the aromatic part.

Based on the previously published assumptions we calculated structure of trianglamine **8**–zinc complex.[20a] For the sake

Table 2 Enantiomeric excesses of the products of asymmetric hydrosilylation of ketones catalyzed by zinc–trianglamine (L*) complexes

Entry	Ar	R	L*	ee[a] [%]
1	4-MeC_6H_4	Me	**8**	98
2	4-MeC_6H_4	Me	**9**	83
3	Ph	Me	**8**	85
4	Ph	Me	**9**	78
5	Ph	Cy	**8**	91
6	Ph	Cy	**9**	84
7	4-NCC_6H_4	Me	**9**	57
8	4-MeOC_6H_4	Me	**8**	70
9	1-Indanone		**8**	87
10	1-Indanone		**9**	97
11	1-Tetralone		**8**	77
12	1-Tetralone		**9**	69
13	Ph	2-MeC_6H_4	**8**	51
14	Ph	2-MeC_6H_4	**9**	73
15	Ph	3-MeC_6H_4	**8**	24
16	Ph	3-MeC_6H_4	**9**	25
17	Ph	4-MeC_6H_4	**8**	21
18	Ph	4-MeC_6H_4	**9**	5
19	Ph	CF_3	**8**	10
20	2,4,6-$Me_3C_6H_2$	CF_3	**8**	4
21	2,4,6-$Me_3C_6H_2$	CF_3	**9**	30

[a] Enantiomeric excesses were determined by HPLC with a CHIRALPAK IA column.

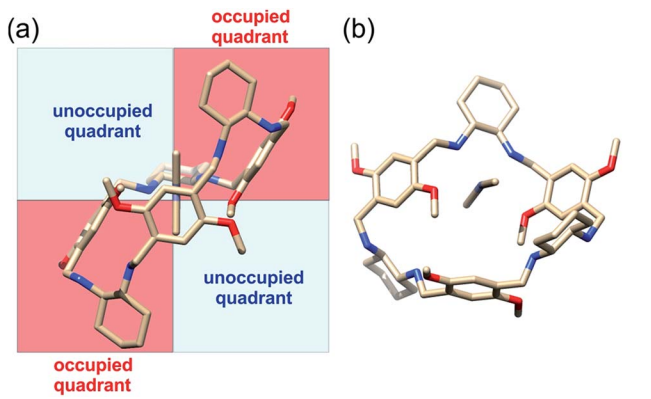

Fig. 8 Calculated at the B3LYP/6-311G(d,p) level folded structure of **8**·Zn(II) shown in two different projections: from side (a) and from the top (b). Colored squares represent occupied (red) and unoccupied (blue) quadrants.

This journal is © The Royal Society of Chemistry 2016

Published on 27 May 2016. Downloaded by UNIVERSITY OF NEBRASKA on 08/06/2016 06:34:59.

of simplicity we replaced diethylzinc by dimethylzinc. From the considered here possible geometries of Zn–**8** complexes, differ in the ligand conformation, the folded one is lower in energy than the fully extended, as revealed by computation at the B3LYP/6-311G(d,p) level. The estimated $\Delta\Delta G$ energy difference between extended form, characterized by all-*trans* arrangement of rotatable torsion angles and the folded one, where some of the torsion angle are in *gauche* conformation is over 6 kcal mol^{-1}.[14,20a] The calculated folded structure of mononuclear [**8**·Zn(II)] complex (shown in Fig. 8) is close to preferred by free trianglamine conformation.[14] The complex consists of two occupied and two unoccupied quadrants, thus, resembles the structure of ruthenium and rhodium species used for asymmetric hydrogenations. The unoccupied quadrants are accessible to approaching substrates and the role of sterical hindrance in the occupied quadrants can be ascribed to two from the three apexes of the triangle. The shielding effect is additionally tuned by the presence of methoxy groups, which explains thereby the relatively low yield of the product.

Conclusions

We presented here synthesis and structural studies on chiral macrocyclic triangular hexaimines and hexaamines. These compounds are readily available through cyclocondensation reaction between optically active vicinal diamines and aromatic aldehydes. The structure and contrasting properties of the product is affected by the nature of substituent in aromatic moiety. Although triangular shape of cycloimination product is not altered, symmetry of the given macrocycle is strongly-substituent-dependent. The 2-nitroterephthaldehyde provide non-symmetrical product, which is apparently formed under kinetic control. The structure of the macrocycle is determined by the structure of reaction intermediates. Energetically preferable symmetrical intermediates provided always non-symmetrical macrocycle.

Contrary, both the symmetrical **5** and non-symmetrical **7** are formed under thermodynamic control. In the last case, the higher-energy C_3-symmetrical isomer is formed as well. The equilibrium between isomers of **7** differ in symmetry did not change upon time. The ^{1}H NMR spectra measured for solution of **7** at the regular time intervals do not show any change in proportion of respective isomers.

For **5** and **7** the structure of the macrocycle is mainly controlled by the tendency to minimization of electrostatic interactions between oxygen and imine nitrogen atoms. Due to the presence of only one methoxy group in each aromatic part of the triangle, the repulsive O···O interactions are responsible for the preference of C_1- over C_3-symmetrical structure of **7**.

The measured ECD spectra of trianglimines **5** and **6** are conveniently interpret using exciton-chirality formalism. The negative exciton couplet is in agreement with negative chirality of N–C*–C*N angle and reflected absolute configuration of the stereogenic centers. The ECD spectrum of macrocycle **5** is exceptional, due to two exciton-type couplets of opposite signs, that resulted from interaction between either electronic transition dipole moments polarised along or perpendicular to the long axis of the chromophore.

The study on chiroptical properties of trianglimine **6** were expanded on vibrational spectroscopy. The most convenient regions for interpreting IR and VCD spectra correspond to N–O asymmetric stretch and C–H bending. Cotton effects associated with C=N absorption are very small due to the mutual cancelation of rotatory strengths of opposite signs.

Suitable substitution pattern allowed tuning of molecular and supramolecular properties of the macrocycle. The presence of electron donating groups in **5** affected its chiroptical properties especially when proton donor is present in solution. Addition of small amounts of acid caused strong bathochromic shift of UV maxima. Color of the solution of **5** changed to deep red during titration. Since **5** is optically active this property may be useful in supramolecular chemistry to construct a new macrocyclic receptors for chiral carboxylic acids. On the other side, the presence of an electron withdrawing group, like nitro, is responsible for unprecedented gelation properties. Due to its efficiency, the nitro-substituted trianglimine may be treated as low molecular weight supergelator,[40] which forms, in polar media, stable chiral organogels at concentration as low as 0.4% m/v. The gelation can be useful for purposes, such as the enantiomeric separation of racemates or chiral recognition. The morphology of the gel is strongly affected by addition of other chiral macrocycle. Whereas for gels made from "pure" **5** the material obtained after drying is amorphous, addition of both enantiomers of **5** to chloroform solution of **6** let to obtain microcrystals after drying.

Despite the symmetry, the reduced trianglamines **8** and **9** originated from **5** and **6**, respectively, are suitable zinc ligands that may be used in asymmetric catalysis. The presence of methoxy group, for instance, increased level of the asymmetric induction in zinc-catalyzed asymmetric hydrosilylation of ketones. The enantiomeric excesses determined for products of AHS reactions, catalyzed by mononuclear **8**·Zn(II) complex reached 98%, which remains the best result obtained for Zn–amine AHS of ketones so far.

The application of trianglamines reported here and similar compounds to other fields of catalytic asymmetric synthesis and to construction of supramolecular assemblies capable of serving certain functions is currently under progress in our laboratory.

Acknowledgements

This work was supported by research grant from National Science Center (NCN) Poland no UMO-2012/06/A/ST5/00230. All calculations were performed in Poznan Supercomputing and Networking Center (grant no. 217). The authors express their gratitude to Dr P. Półrolniczak (Institute of Non-Ferrous Metals, Division in Poznań) and Dr Ł. Majchrzycki (WCAT) for their attempts to take powder X-ray diffraction, SEM and AFM measurements.

Notes and references

1 N. E. Borisova, M. D. Reshetova and Y. A. Ustynyuk, *Chem. Rev.*, 2007, **107**, 46.

Published on 27 May 2016. Downloaded by UNIVERSITY OF NEBRASKA on 08/06/2016 06:34:59.

2 S. J. Lee and W. Lin, Chiral Macrocycles, in *Encyclopedia of Nanoscience and Nanotechnology*, ed. H. S. Nalwa, American Scientific Publishers, 2004, vol. 1, pp. 863–875.
3 S. Srimurugan, P. Suresh, B. Babu and H. N. Pati, *Mini-Rev. Org. Chem.*, 2008, **5**, 228.
4 J. Gawroński, H. Kołbon, M. Kwit and A. Katrusiak, *J. Org. Chem.*, 2000, **65**, 5768.
5 M. Chadim, M. Buděšínský, J. Hodačová, J. Závada and P. C. Junk, *Tetrahedron: Asymmetry*, 2001, **12**, 127.
6 N. Kuhnert, C. Straßnig and A. M. Lopez-Periago, *Tetrahedron: Asymmetry*, 2002, **13**, 123.
7 N. Kuhnert and A. M. Lopez-Periago, *Tetrahedron Lett.*, 2002, **43**, 3329.
8 For the use of DACH as chiral scaffold see: Y. L. Bennani and S. Hanessian, *Chem. Rev.*, 1997, **97**, 3161.
9 (*a*) N. Kuhnert, A. Lopez-Periago and G. M. Rossignolo, *Org. Biomol. Chem.*, 2005, **3**, 524; (*b*) H. F. Nour, M. F. Matei, B. S. Bassil, U. Kortz and N. Kuhnert, *Org. Biomol. Chem.*, 2011, **9**, 3258.
10 (*a*) S.-K. Lin, *J. Chem. Inf. Comput. Sci.*, 1996, **36**, 367; (*b*) J. Rosen, *Entropy*, 2005, **7**, 308; (*c*) S.-K. Lin, *Int. J. Mol. Sci.*, 2001, **2**, 10.
11 P. Skowronek, B. Warżajtis, U. Rychlewska and J. Gawroński, *Chem. Commun.*, 2013, **49**, 2524.
12 S. W. Sisco and J. S. Moore, *Chem. Sci.*, 2014, **5**, 81.
13 K. Tanaka, S. Fukuoka, H. Miyanishi and H. Takahashi, *Tetrahedron Lett.*, 2010, **51**, 2693.
14 J. Gawroński, K. Gawrońska, J. Grajewski, M. Kwit, A. Plutecka and U. Rychlewska, *Chem.–Eur. J.*, 2006, **12**, 1807.
15 (*a*) N. Kuhnert, D. Marsh and D. C. Nicolau, *Tetrahedron: Asymmetry*, 2007, **18**, 1648; (*b*) K. Tanaka, N. Fukuda and T. Fujiwara, *Tetrahedron: Asymmetry*, 2007, **18**, 2657; (*c*) M. Periasamy, M. Dalai and M. Padmaja, *J. Chem. Sci.*, 2010, **122**, 561; (*d*) A. Gualandi, S. Grilli, D. Savoia, M. Kwit and J. Gawroński, *Org. Biomol. Chem.*, 2011, **9**, 4234.
16 (*a*) J. Gao and A. E. Martell, *Org. Biomol. Chem.*, 2003, **1**, 2801; (*b*) J. Gao and A. E. Martell, *Org. Biomol. Chem.*, 2003, **1**, 2795; (*c*) K. Tanaka and S. Hachiken, *Tetrahedron Lett.*, 2008, **49**, 2533; (*d*) K. Tanaka, A. Asakura, T. Muraoka, P. Kalicki and Z. Urbanczyk-Lipkowska, *New J. Chem.*, 2013, **37**, 2851.
17 H. Mimoun, J. Y. de Saint Laumer, L. Giannini, R. Scopelliti and C. Floriani, *J. Am. Chem. Soc.*, 1999, **121**, 6158.
18 For application of zinc in asymmetric catalysis see, for example: (*a*) D. Łowicki, S. Baś and J. Mlynarski, *Tetrahedron*, 2015, **71**, 1339; (*b*) S. Enthaler, *ACS Catal.*, 2013, **3**, 150.
19 (*a*) H. Ushio and K. Mikami, *Tetrahedron Lett.*, 2005, **46**, 2903; (*b*) V. Bette, A. Mortreux, D. Savoia and J.-F. Carpentier, *Tetrahedron*, 2004, **60**, 2837; (*c*) V. Bette, A. Mortreux, F. Ferioli, G. Martelli, D. Savoia and J.-F. Carpentier, *Eur. J. Org. Chem.*, 2004, 3040; (*d*) V. Bette, A. Mortreux, C. W. Lehmann and J.-F. Carpentier, *Chem. Commun.*, 2003, 332; (*e*) V. Bette, A. Mortreux, D. Savoia and J.-F. Carpentier, *Adv. Synth. Catal.*, 2005, **347**, 289.
20 (*a*) J. Gajewy, M. Kwit and J. Gawroński, *Adv. Synth. Catal.*, 2009, **351**, 1055; (*b*) J. Gajewy, J. Gawronski and M. Kwit, *Monatsh. Chem.*, 2012, **143**, 1045; (*c*) D. Savoia, A. Gualandi and H. Stoeckli-Evans, *Org. Biomol. Chem.*, 2010, **8**, 3992.
21 J. Gajewy, J. Gawronski and M. Kwit, *Org. Biomol. Chem.*, 2011, **9**, 3863.
22 M. Szewczyk, F. Stanek, A. Bezłada and J. Młynarski, *Adv. Synth. Catal.*, 2015, **357**, 3727.
23 N. Kuhnert, G. M. Rossignolo and A. Lopez-Periago, *Org. Biomol. Chem.*, 2003, **1**, 1157.
24 A. M. Piggott and P. Karuso, *Tetrahedron Lett.*, 2005, **46**, 8241.
25 D. T. B. Hannah and D. C. Sherrington, *J. Mater. Chem.*, 1997, **7**, 1985.
26 Scigress 2.5, Fujitsu Ltd.
27 M. J. Frisch, G. W. Trucks, H. B. Schlegel, G. E. Scuseria, M. A. Robb, J. R. Cheeseman, G. Scalmani, V. Barone, B. Mennucci, G. A. Petersson, H. Nakatsuji, M. Caricato, X. Li, H. P. Hratchian, A. F. Izmaylov, J. Bloino, G. Zheng, J. L. Sonnenberg, M. Hada, M. Ehara, K. Toyota, R. Fukuda, J. Hasegawa, M. Ishida, T. Nakajima, Y. Honda, O. Kitao, H. Nakai, T. Vreven, J. A. Montgomery Jr, J. E. Peralta, F. Ogliaro, M. Bearpark, J. J. Heyd, E. Brothers, K. N. Kudin, V. N. Staroverov, R. Kobayashi, J. Normand, K. Raghavachari, A. Rendell, J. C. Burant, S. S. Iyengar, J. Tomasi, M. Cossi, N. Rega, N. J. Millam, M. Klene, J. E. Knox, J. B. Cross, V. Bakken, C. Adamo, J. Jaramillo, R. Gomperts, R. E. Stratmann, O. Yazyev, A. J. Austin, R. Cammi, C. Pomelli, J. W. Ochterski, R. L. Martin, K. Morokuma, V. G. Zakrzewski, G. A. Voth, P. Salvador, J. J. Dannenberg, S. Dapprich, A. D. Daniels, Ö. Farkas, J. B. Foresman, J. V. Ortiz, J. Cioslowski and D. J. Fox, *Gaussian 09, revision A.02*, Gaussian, Inc., Wallingford CT, 2009.
28 M. Kwit, M. D. Rozwadowska, J. Gawronski and A. Grajewska, *J. Org. Chem.*, 2009, **74**, 8051 and references therein.
29 T. Yanai, D. Tew and N. Handy, *Chem. Phys. Lett.*, 2004, **393**, 51.
30 (*a*) Y. Zhao and D. G. Truhlar, *Theor. Chem. Acc.*, 2008, **120**, 215; (*b*) D. Jacquemin, E. A. Perpète, I. Ciofini, C. Adamo, R. Valero, Y. Zhao and D. G. Truhlar, *J. Chem. Theory Comput.*, 2010, **6**, 2071.
31 (*a*) S. Grimme, *J. Chem. Phys.*, 2006, **124**, 034108; (*b*) L. Goerigk and S. Grimme, *J. Phys. Chem. A*, 2009, **113**, 767.
32 (*a*) C. Adamo and V. Barone, *J. Chem. Phys.*, 1999, **110**, 6158; (*b*) Y. Tawada, T. Tsuneda, S. Yanagisawa, T. Yanai and K. Hirao, *J. Chem. Phys.*, 2004, **120**, 8425.
33 (*a*) N. Prusinowska, W. Bendzińska-Berus, M. Jelecki, U. Rychlewska and M. Kwit, *Eur. J. Org. Chem.*, 2015, 738; (*b*) N. Prusinowska, W. Bendzińska-Berus, J. Szymkowiak, B. Warżajtis, J. Gajewy, M. Jelecki, U. Rychlewska and M. Kwit, *RSC Adv.*, 2015, **5**, 83448.
34 N. Harada and P. Stephens, *Chirality*, 2010, **22**, 229.
35 P. J. Stephens, F. J. Devlin and J. R. Cheeseman, *VCD Spectroscopy for Organic Chemists*, CRC Press, Boca Raton, 2012.
36 H. F. Nour, A. M. Lopez-Periago and N. Kuhnert, *Rapid Commun. Mass Spectrom.*, 2012, **26**, 1070.

 This journal is © The Royal Society of Chemistry 2016

37 N. Harada and K. Nakanishi, *Circularly Dichroic Spectroscopy – Exciton Coupling in Organic Stereochemistry*, University Science Books, Mill Valley, 1983.
38 Similar effect was previously reported by Gawroński *et al.* for ECD spectra of chiral 1,8-naphthalimides, see: P. Skowronek and J. Gawroński, *Curr. Org. Chem.*, 2004, **8**, 65 and literature therein.
39 (*a*) D. Łowicki, A. Bezłada and J. Młynarski, *Adv. Synth. Catal.*, 2014, **356**, 591; (*b*) A. Bezłada, M. Szewczyk and J. Młynarski, *J. Org. Chem.*, 2016, **81**, 336.
40 (*a*) P. Terech and R. G. Weiss, *Chem. Rev.*, 1997, **97**, 3133; (*b*) D. J. Abdallah and R. G. Weiss, *Adv. Mater.*, 2000, **12**, 1237.

Published on 27 May 2016. Downloaded by UNIVERSITY OF NEBRASKA on 08/06/2016 06:34:59.